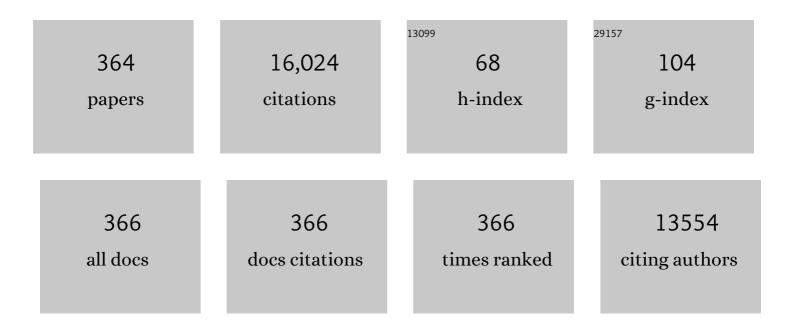
List of Publications by Year in descending order

Source: https://exaly.com/author-pdf/2485877/publications.pdf Version: 2024-02-01



SHENC-LIZHU

#	Article	IF	CITATIONS
1	Amorphous Metallic NiFeP: A Conductive Bulk Material Achieving High Activity for Oxygen Evolution Reaction in Both Alkaline and Acidic Media. Advanced Materials, 2017, 29, 1606570.	21.0	441
2	Rapid Biofilm Eradication on Bone Implants Using Red Phosphorus and Nearâ€Infrared Light. Advanced Materials, 2018, 30, e1801808.	21.0	364
3	Zinc-doped Prussian blue enhances photothermal clearance of Staphylococcus aureus and promotes tissue repair in infected wounds. Nature Communications, 2019, 10, 4490.	12.8	306
4	Repeatable Photodynamic Therapy with Triggered Signaling Pathways of Fibroblast Cell Proliferation and Differentiation To Promote Bacteria-Accompanied Wound Healing. ACS Nano, 2018, 12, 1747-1759.	14.6	303
5	Interfacial engineering of Bi2S3/Ti3C2Tx MXene based on work function for rapid photo-excited bacteria-killing. Nature Communications, 2021, 12, 1224.	12.8	283
6	The recent progress on metal–organic frameworks for phototherapy. Chemical Society Reviews, 2021, 50, 5086-5125.	38.1	262
7	Enhanced photocatalytic activity and photothermal effects of cu-doped metal-organic frameworks for rapid treatment of bacteria-infected wounds. Applied Catalysis B: Environmental, 2020, 261, 118248.	20.2	255
8	Tuning the Bandgap of Photo-Sensitive Polydopamine/Ag <sub>3</sub> PO <sub>4</sub> /Graphene Oxide Coating for Rapid, Noninvasive Disinfection of Implants. ACS Central Science, 2018, 4, 724-738.	11.3	227
9	Highly Effective and Noninvasive Nearâ€Infrared Eradication of a <i>Staphylococcus aureus</i> Biofilm on Implants by a Photoresponsive Coating within 20 Min. Advanced Science, 2019, 6, 1900599.	11.2	212
10	Nanoporous Palladium Hydride for Electrocatalytic N <sub>2</sub> Reduction under Ambient Conditions. Angewandte Chemie - International Edition, 2020, 59, 3511-3516.	13.8	182
11	Rapid Photo-Sonotherapy for Clinical Treatment of Bacterial Infected Bone Implants by Creating Oxygen Deficiency Using Sulfur Doping. ACS Nano, 2020, 14, 2077-2089.	14.6	182
12	Controlled-temperature photothermal and oxidative bacteria killing and acceleration of wound healing by polydopamine-assisted Au-hydroxyapatite nanorods. Acta Biomaterialia, 2018, 77, 352-364.	8.3	180
13	Rapid and Superior Bacteria Killing of Carbon Quantum Dots/ZnO Decorated Injectable Folic Acidâ€Conjugated PDA Hydrogel through Dual‣ight Triggered ROS and Membrane Permeability. Small, 2019, 15, e1900322.	10.0	180
14	A new Ti-based bulk glassy alloy with potential for biomedical application. Materials Science & Engineering A: Structural Materials: Properties, Microstructure and Processing, 2007, 459, 233-237.	5.6	172
15	Treatment of MRSA-infected osteomyelitis using bacterial capturing, magnetically targeted composites with microwave-assisted bacterial killing. Nature Communications, 2020, 11, 4446.	12.8	165
16	2D MOF Periodontitis Photodynamic Ion Therapy. Journal of the American Chemical Society, 2021, 143, 15427-15439.	13.7	161
17	Study on corrosion properties of pipelines in simulated produced water saturated with supercritical CO2. Applied Surface Science, 2006, 252, 2368-2374.	6.1	154
18	Local Photothermal/Photodynamic Synergistic Therapy by Disrupting Bacterial Membrane To Accelerate Reactive Oxygen Species Permeation and Protein Leakage. ACS Applied Materials & Interfaces, 2019, 11, 17902-17914.	8.0	149

#	Article	IF	CITATIONS
19	Single-Atom Catalysis for Efficient Sonodynamic Therapy of Methicillin-Resistant <i>Staphylococcus aureus</i> -Infected Osteomyelitis. ACS Nano, 2021, 15, 10628-10639.	14.6	144
20	Rapid bacteria trapping and killing of metal-organic frameworks strengthened photo-responsive hydrogel for rapid tissue repair of bacterial infected wounds. Chemical Engineering Journal, 2020, 396, 125194.	12.7	142
21	Eradicating Multidrugâ€Resistant Bacteria Rapidly Using a Multi Functional g <sub>3</sub> N <sub>4</sub> @ Bi <sub>2</sub> S <sub>3</sub> Nanorod Heterojunction with or without Antibiotics. Advanced Functional Materials, 2019, 29, 1900946.	14.9	136
22	Near-Infrared Light Triggered Phototherapy and Immunotherapy for Elimination of Methicillin-Resistant <i>Staphylococcus aureus</i> Biofilm Infection on Bone Implant. ACS Nano, 2020, 14, 8157-8170.	14.6	133
23	Synthesis of Cu <sub>2</sub> 0 Octadecahedron/TiO <sub>2</sub> Quantum Dot Heterojunctions with High Visible Light Photocatalytic Activity and High Stability. ACS Applied Materials & Interfaces, 2016, 8, 91-101.	8.0	132
24	Glass-forming ability and mechanical properties of Ti-based bulk glassy alloys with large diameters of up to 1cm. Intermetallics, 2008, 16, 1031-1035.	3.9	129
25	Nano Ag/ZnO-Incorporated Hydroxyapatite Composite Coatings: Highly Effective Infection Prevention and Excellent Osteointegration. ACS Applied Materials & amp; Interfaces, 2018, 10, 1266-1277.	8.0	127
26	Defect enhances photocatalytic activity of ultrathin TiO2 (B) nanosheets for hydrogen production by plasma engraving method. Applied Catalysis B: Environmental, 2018, 230, 11-17.	20.2	125
27	The enhanced photocatalytic properties of MnO2/g-C3N4 heterostructure for rapid sterilization under visible light. Journal of Hazardous Materials, 2019, 377, 227-236.	12.4	122
28	Silver nanoparticles supported on TiO2 nanotubes as active catalysts for ethanol oxidation. Journal of Catalysis, 2011, 278, 276-287.	6.2	121
29	Nanoporous CuS with excellent photocatalytic property. Scientific Reports, 2016, 5, 18125.	3.3	117
30	Incorporation of silver and strontium in hydroxyapatite coating on titanium surface for enhanced antibacterial and biological properties. Materials Science and Engineering C, 2017, 71, 852-861.	7.3	116
31	Visible light responsive CuS/ protonated g-C3N4 heterostructure for rapid sterilization. Journal of Hazardous Materials, 2020, 393, 122423.	12.4	116
32	Design of a highly sensitive ethanol sensor using a nano-coaxial p-Co3O4/n-TiO2 heterojunction synthesized at low temperature. Nanoscale, 2013, 5, 10916.	5.6	113
33	Stress–strain behavior of porous NiTi alloys prepared by powders sintering. Materials Science & Engineering A: Structural Materials: Properties, Microstructure and Processing, 2005, 408, 264-268.	5.6	108
34	Dual Metal–Organic Framework Heterointerface. ACS Central Science, 2019, 5, 1591-1601.	11.3	108
35	A nanoporous metal phosphide catalyst for bifunctional water splitting. Journal of Materials Chemistry A, 2018, 6, 5574-5579.	10.3	106
36	Ni <sub>2</sub> P nanoflakes for the high-performing urea oxidation reaction: linking active sites to a UOR mechanism. Nanoscale, 2021, 13, 1759-1769.	5.6	106

#	Article	IF	CITATIONS
37	Antibacterial Hybrid Hydrogels. Macromolecular Bioscience, 2021, 21, e2000252.	4.1	105
38	Enhanced photocatalytic and photothermal properties of ecofriendly metal-organic framework heterojunction for rapid sterilization. Chemical Engineering Journal, 2021, 405, 126730.	12.7	104
39	Electronic Structure Modulation of Nanoporous Cobalt Phosphide by Carbon Doping for Alkaline Hydrogen Evolution Reaction. Advanced Functional Materials, 2021, 31, 2107333.	14.9	104
40	Characterization of the surface film formed from carbon dioxide corrosion on N80 steel. Materials Letters, 2004, 58, 1076-1081.	2.6	102
41	Synthesis of three-dimensionally ordered macroporous LaFeO3 with enhanced methanol gas sensing properties. Sensors and Actuators B: Chemical, 2015, 209, 706-713.	7.8	102
42	Photoresponsive Materials for Antibacterial Applications. Cell Reports Physical Science, 2020, 1, 100245.	5.6	102
43	Recent Progress in Photocatalytic Antibacterial. ACS Applied Bio Materials, 2021, 4, 3909-3936.	4.6	100
44	Ultrasonic Interfacial Engineering of Red Phosphorous–Metal for Eradicating MRSA Infection Effectively. Advanced Materials, 2021, 33, e2006047.	21.0	93
45	Study on the formation of an apatite layer on NiTi shape memory alloy using a chemical treatment method. Surface and Coatings Technology, 2003, 173, 229-234.	4.8	91
46	Strontium incorporation to optimize the antibacterial and biological characteristics of silver-substituted hydroxyapatite coating. Materials Science and Engineering C, 2016, 58, 467-477.	7.3	91
47	Photothermy-strengthened photocatalytic activity of polydopamine-modified metal-organic frameworks for rapid therapy of bacteria-infected wounds. Journal of Materials Science and Technology, 2021, 62, 83-95.	10.7	91
48	Self-supported Ni3Se2@NiFe layered double hydroxide bifunctional electrocatalyst for overall water splitting. Journal of Colloid and Interface Science, 2021, 587, 79-89.	9.4	89
49	An Engineered Pseudoâ€Macrophage for Rapid Treatment of Bacteriaâ€Infected Osteomyelitis via Microwaveâ€Excited Antiâ€Infection and Immunoregulation. Advanced Materials, 2021, 33, e2102926.	21.0	87
50	Rapid and Highly Effective Noninvasive Disinfection by Hybrid Ag/CS@MnO <sub>2</sub> Nanosheets Using Near-Infrared Light. ACS Applied Materials & Interfaces, 2019, 11, 15014-15027.	8.0	86
51	Effect of Zr on super-elasticity and mechanical properties of Ti–24at% Nb–(0, 2, 4)at% Zr alloy subjected to aging treatment. Materials Science & Engineering A: Structural Materials: Properties, Microstructure and Processing, 2012, 536, 197-206.	5.6	85
52	Superimposed surface plasma resonance effect enhanced the near-infrared photocatalytic activity of Au@Bi2WO6 coating for rapid bacterial killing. Journal of Hazardous Materials, 2019, 380, 120818.	12.4	85
53	Ag3PO4 decorated black urchin-like defective TiO2 for rapid and long-term bacteria-killing under visible light. Bioactive Materials, 2021, 6, 1575-1587.	15.6	85
54	Processing of porous TiNi shape memory alloy from elemental powders by Ar-sintering. Materials Letters, 2004, 58, 2369-2373.	2.6	84

#	Article	IF	CITATIONS
55	Synthesis and properties of morphology controllable copper sulphide nanosheets for supercapacitor application. Electrochimica Acta, 2016, 211, 891-899.	5.2	84
56	Synthesis and properties of nanoporous Ag2S/CuS catalyst for hydrogen evolution reaction. Electrochimica Acta, 2016, 190, 221-228.	5.2	82
57	Engineered probiotics biofilm enhances osseointegration via immunoregulation and anti-infection. Science Advances, 2020, 6, .	10.3	82
58	EIS study of the surface film on the surface of carbon steel from supercritical carbon dioxide corrosion. Applied Surface Science, 2004, 228, 17-25.	6.1	77
59	Na+ inserted metal-organic framework for rapid therapy of bacteria-infected osteomyelitis through microwave strengthened Fenton reaction and thermal effects. Nano Today, 2021, 37, 101090.	11.9	77
60	Self-activating anti-infection implant. Nature Communications, 2021, 12, 6907.	12.8	77
61	Controlled release behaviour and antibacterial effects of antibiotic-loaded titania nanotubes. Materials Science and Engineering C, 2016, 62, 105-112.	7.3	76
62	An amorphous nanoporous PdCuNi-S hybrid electrocatalyst for highly efficient hydrogen production. Applied Catalysis B: Environmental, 2019, 246, 156-165.	20.2	75
63	Lysozyme-Assisted Photothermal Eradication of Methicillin-Resistant <i>Staphylococcus aureus</i> Infection and Accelerated Tissue Repair with Natural Melanosome Nanostructures. ACS Nano, 2019, 13, 11153-11167.	14.6	74
64	A Z-scheme heterojunction of ZnO/CDots/C3N4 for strengthened photoresponsive bacteria-killing and acceleration of wound healing. Journal of Materials Science and Technology, 2020, 57, 1-11.	10.7	74
65	Microstructure and wear performance of gradient Ti/TiN metal matrix composite coating synthesized using a gas nitriding technology. Surface and Coatings Technology, 2005, 190, 309-313.	4.8	73
66	Pd coated MoS 2 nanoflowers for highly efficient hydrogen evolution reaction under irradiation. Journal of Power Sources, 2015, 284, 68-76.	7.8	73
67	In-situ sulfuration of Cu-based metal-organic framework for rapid near-infrared light sterilization. Journal of Hazardous Materials, 2020, 390, 122126.	12.4	72
68	Soft magnetic Fe-Co-based amorphous alloys with extremely high saturation magnetization exceeding 1.9ÂT and low coercivity of 2ÂA/m. Journal of Alloys and Compounds, 2017, 723, 376-384.	5.5	71
69	Rapid Biofilm Elimination on Bone Implants Using Nearâ€Infraredâ€Activated Inorganic Semiconductor Heterostructures. Advanced Healthcare Materials, 2019, 8, e1900835.	7.6	71
70	Designing Highly Efficient and Longâ€Term Durable Electrocatalyst for Oxygen Evolution by Coupling B and P into Amorphous Porous NiFeâ€Based Material. Small, 2019, 15, e1901020.	10.0	71
71	Excellent soft magnetic Fe-Co-B-based amorphous alloys with extremely high saturation magnetization above 1.85ÂT and low coercivity below 3ÂA/m. Journal of Alloys and Compounds, 2017, 711, 132-142.	5.5	70
72	A highly efficient electrocatalyst based on amorphous Pd–Cu–S material for hydrogen evolution reaction. Journal of Materials Chemistry A, 2017, 5, 18793-18800.	10.3	70

#	Article	IF	CITATIONS
73	The enhanced near-infrared photocatalytic and photothermal effects of MXene-based heterojunction for rapid bacteria-killing. Applied Catalysis B: Environmental, 2021, 297, 120500.	20.2	68
74	Ag <sub>2</sub> S@WS <sub>2</sub> Heterostructure for Rapid Bacteria-Killing Using Near-Infrared Light. ACS Sustainable Chemistry and Engineering, 2019, 7, 14982-14990.	6.7	67
75	Lightâ€Activated Rapid Disinfection by Accelerated Charge Transfer in Red Phosphorus/ZnO Heterointerface. Small Methods, 2019, 3, 1900048.	8.6	64
76	Nanoporous NiSb to Enhance Nitrogen Electroreduction via Tailoring Competitive Adsorption Sites. Advanced Materials, 2021, 33, e2101126.	21.0	64
77	Synthesis, characterization and the formation mechanism of magnesium- and strontium-substituted hydroxyapatite. Journal of Materials Chemistry B, 2015, 3, 3738-3746.	5.8	63
78	Ni-free Ti-based bulk metallic glass with potential for biomedical applications produced by spark plasma sintering. Intermetallics, 2012, 29, 99-103.	3.9	61
79	Ce and Er Co-doped TiO2 for rapid bacteria- killing using visible light. Bioactive Materials, 2020, 5, 201-209.	15.6	61
80	Flower-like CuS/graphene oxide with photothermal and enhanced photocatalytic effect for rapid bacteria-killing using visible light. Rare Metals, 2022, 41, 639-649.	7.1	61
81	Photo-Sono Interfacial Engineering Exciting the Intrinsic Property of Herbal Nanomedicine for Rapid Broad-Spectrum Bacteria Killing. ACS Nano, 2021, 15, 18505-18519.	14.6	61
82	Free-standing amorphous nanoporous nickel cobalt phosphide prepared by electrochemically delloying process as a high performance energy storage electrode material. Energy Storage Materials, 2019, 17, 300-308.	18.0	60
83	Three-dimensionally ordered macroporous La 1â^' x Mg x FeO 3 as high performance gas sensor to methanol. Journal of Alloys and Compounds, 2015, 635, 194-202.	5.5	59
84	Corrosion behavior of oil tube steels under conditions of multiphase flow saturated with super-critical carbon dioxide. Materials Letters, 2004, 58, 1035-1040.	2.6	58
85	High entropy effect on structure and properties of (Fe,Co,Ni,Cr)-B amorphous alloys. Journal of Alloys and Compounds, 2017, 696, 345-352.	5.5	58
86	AgBr Nanoparticles in Situ Growth on 2D MoS <sub>2</sub> Nanosheets for Rapid Bacteria-Killing and Photodisinfection. ACS Applied Materials & Interfaces, 2019, 11, 34364-34375.	8.0	58
87	The rapid photoresponsive bacteria-killing of Cu-doped MoS <sub>2</sub> . Biomaterials Science, 2020, 8, 4216-4224.	5.4	57
88	Synthesis of nanoporous CuO/TiO2/Pd-NiO composite catalysts by chemical dealloying and their performance for methanol and ethanol electro-oxidation. Journal of Power Sources, 2017, 362, 10-19.	7.8	56
89	Nanocrystallization, good soft magnetic properties and ultrahigh mechanical strength for Fe82-85B13-16Si1Cu1 amorphous alloys. Journal of Alloys and Compounds, 2019, 785, 25-37.	5.5	56
90	Noble metal-based nanomaterials as antibacterial agents. Journal of Alloys and Compounds, 2022, 904, 164091.	5.5	56

6

#	Article	IF	CITATIONS
91	Near-infrared light photocatalysis and photothermy of carbon quantum dots and au nanoparticles loaded titania nanotube array. Materials and Design, 2019, 177, 107845.	7.0	55
92	Near-infrared light controlled fast self-healing protective coating on magnesium alloy. Corrosion Science, 2020, 163, 108257.	6.6	55
93	One-step synthesis of Mo and S co-doped porous g-C3N4 nanosheets for efficient visible-light photocatalytic hydrogen evolution. Applied Surface Science, 2021, 536, 147743.	6.1	55
94	Preparation of copper-coated $\hat{l}^2$ -SiC nanoparticles by electroless plating. Surface and Coatings Technology, 2011, 205, 2985-2988.	4.8	53
95	Eco-friendly Hybrids of Carbon Quantum Dots Modified MoS <sub>2</sub> for Rapid Microbial Inactivation by Strengthened Photocatalysis. ACS Sustainable Chemistry and Engineering, 2020, 8, 534-542.	6.7	53
96	Rapid Sterilization by Photocatalytic Ag <sub>3</sub> PO <sub>4</sub> /α-Fe <sub>2</sub> O <sub>3</sub> Composites Using Visible Light. ACS Sustainable Chemistry and Engineering, 2020, 8, 2577-2585.	6.7	53
97	An UV to NIR-driven platform based on red phosphorus/graphene oxide film for rapid microbial inactivation. Chemical Engineering Journal, 2020, 383, 123088.	12.7	52
98	In situ synthesis of a novel Mn3O4/g-C3N4 p-n heterostructure photocatalyst for water splitting. Journal of Colloid and Interface Science, 2021, 586, 778-784.	9.4	52
99	MoO <sub>2</sub> –CoO coupled with a macroporous carbon hybrid electrocatalyst for highly efficient oxygen evolution. Nanoscale, 2015, 7, 16704-16714.	5.6	51
100	3D microporous Co3O4-carbon hybrids biotemplated from butterfly wings as high performance VOCs gas sensor. Sensors and Actuators B: Chemical, 2016, 235, 420-431.	7.8	51
101	Photoelectric-Responsive Extracellular Matrix for Bone Engineering. ACS Nano, 2019, 13, 13581-13594.	14.6	51
102	Modulation of the mechanosensing of mesenchymal stem cells by laser-induced patterning for the acceleration of tissue reconstruction through the Wnt/β-catenin signaling pathway activation. Acta Biomaterialia, 2020, 101, 152-167.	8.3	51
103	Photoelectrons Mediating Angiogenesis and Immunotherapy through Heterojunction Film for Noninvasive Disinfection. Advanced Science, 2020, 7, 2000023.	11.2	51
104	New TiZrCuPd Quaternary Bulk Glassy Alloys with Potential of Biomedical Applications. Materials Transactions, 2007, 48, 2445-2448.	1.2	50
105	Extraordinary Supercapacitor Performance of a Multicomponent and Mixedâ€Valence Oxyhydroxide. Angewandte Chemie - International Edition, 2015, 54, 8100-8104.	13.8	50
106	Corrosion Behavior of a Ti-Based Bulk Metallic Glass and Its Crystalline Alloys. Materials Transactions, 2007, 48, 1855-1858.	1.2	49
107	Production methods and properties of engineering glassy alloys and composites. Intermetallics, 2015, 58, 20-30.	3.9	49
108	Development and application of Fe-based soft magnetic bulk metallic glassy inductors. Journal of Alloys and Compounds, 2018, 731, 1303-1309.	5.5	49

#	Article	IF	CITATIONS
109	Overcoming Multidrugâ€Resistant MRSA Using Conventional Aminoglycoside Antibiotics. Advanced Science, 2020, 7, 1902070.	11.2	49
110	High-performance five-ring-fused organic semiconductors for field-effect transistors. Chemical Society Reviews, 2022, 51, 3071-3122.	38.1	49
111	Microwave assisted antibacterial action of Garcinia nanoparticles on Gram-negative bacteria. Nature Communications, 2022, 13, 2461.	12.8	49
112	Ti oxide nano-porous surface structure prepared by dealloying of Ti–Cu amorphous alloy. Electrochemistry Communications, 2011, 13, 250-253.	4.7	48
113	FeCo-based soft magnetic alloys with high Bs approaching 1.75ÂTÂandÂgood bending ductility. Journal of Alloys and Compounds, 2017, 691, 364-368.	5.5	48
114	Corrosion behavior and mechanical properties of Mg–Zn–Ca amorphous alloys. Intermetallics, 2013, 42, 9-13.	3.9	47
115	The enhanced photocatalytic sterilization of MOF-Based nanohybrid for rapid and portable therapy of bacteria-infected open wounds. Bioactive Materials, 2022, 13, 200-211.	15.6	47
116	Syntheses and corrosion behaviors of Fe-based amorphous soft magnetic alloys with high-saturation magnetization near 1.7 T. Journal of Materials Research, 2015, 30, 547-555.	2.6	46
117	A Bi <sub>2</sub> Te <sub>3</sub> @CoNiMo composite as a high performance bifunctional catalyst for hydrogen and oxygen evolution reactions. Journal of Materials Chemistry A, 2015, 3, 22770-22780.	10.3	46
118	Formation, thermal stability and mechanical properties of high entropy (Fe,Co,Ni,Cr,Mo)-B amorphous alloys. Journal of Alloys and Compounds, 2018, 732, 637-645.	5.5	46
119	Synthesis of CuO/Co <sub>3</sub> O <sub>4</sub> Coaxial Heterostructures for Efficient and Recycling Photodegradation. International Journal of Photoenergy, 2015, 2015, 1-11.	2.5	45
120	Structure engineering of electrodeposited NiMoÂfilms for highly efficient and durable seawater splitting. Electrochimica Acta, 2021, 365, 137366.	5.2	45
121	Fabrication and Corrosion Property of Novel Ti-Based Bulk Glassy Alloys without Ni. Materials Transactions, 2007, 48, 515-518.	1.2	44
122	Ag2S decorated nanocubes with enhanced near-infrared photothermal and photodynamic properties for rapid sterilization. Colloids and Interface Science Communications, 2019, 33, 100201.	4.1	44
123	Rapid bacteria capturing and killing by AgNPs/N-CD@ZnO hybrids strengthened photo-responsive xerogel for rapid healing of bacteria-infected wounds. Chemical Engineering Journal, 2021, 414, 128805.	12.7	44
124	Influence of Zr content on phase transformation, microstructure and mechanical properties of Ti75â^'xNb25Zrx (x=0–6) alloys. Journal of Alloys and Compounds, 2009, 486, 628-632.	5.5	43
125	Synthesis of α-Fe2O3/g-C3N4 photocatalyst for high-efficiency water splitting under full light. Materials and Design, 2020, 196, 109191.	7.0	43
126	Formation, stability and ultrahigh strength of novel nanostructured alloys by partial crystallization of high-entropy (Fe0.25Co0.25Ni0.25Cr0.125Mo0.125)86‒89B11‒14 amorphous phase. Acta Materialia, 20 170, 50-61.	)197,9	42

#	Article	IF	CITATIONS
127	Highly efficient nanoporous CoBP electrocatalyst for hydrogen evolution reaction. Rare Metals, 2021, 40, 1031-1039.	7.1	42
128	Simultaneously enhancing the photocatalytic and photothermal effect of NH2-MIL-125-GO-Pt ternary heterojunction for rapid therapy of bacteria-infected wounds. Bioactive Materials, 2022, 18, 421-432.	15.6	42
129	New Fe-based soft magnetic amorphous alloys with high saturation magnetization and good corrosion resistance for dust core application. Intermetallics, 2016, 76, 18-25.	3.9	41
130	Zn2+-assisted photothermal therapy for rapid bacteria-killing using biodegradable humic acid encapsulated MOFs. Colloids and Surfaces B: Biointerfaces, 2020, 188, 110781.	5.0	41
131	Sandwich structured Ni3S2-MoS2-Ni3S2@Ni foam electrode as a stable bifunctional electrocatalyst for highly sustained overall seawater splitting. Electrochimica Acta, 2021, 390, 138833.	5.2	41
132	Recent Progress in Ti-Based Metallic Glasses for Application as Biomaterials. Materials Transactions, 2013, 54, 1314-1323.	1.2	40
133	Corrosion behaviour of porous Ni-free Ti-based bulk metallic glass produced by spark plasma sintering in Hanks' solution. Intermetallics, 2014, 44, 55-59.	3.9	40
134	Self-supporting amorphous nanoporous NiFeCoP electrocatalyst for efficient overall water splitting. Journal of Materials Science and Technology, 2021, 82, 96-104.	10.7	40
135	The synergistic effect of strontium-substituted hydroxyapatite and microRNA-21 on improving bone remodeling and osseointegration. Biomaterials Science, 2018, 6, 2694-2703.	5.4	39
136	Two-Dimensional Lamellar Mo <sub>2</sub> C for Electrochemical Hydrogen Production: Insights into the Origin of Hydrogen Evolution Reaction Activity in Acidic and Alkaline Electrolytes. ACS Applied Materials & Interfaces, 2018, 10, 40500-40508.	8.0	38
137	Unraveling the osteogenesis of magnesium by the activity of osteoblasts <i>in vitro</i> . Journal of Materials Chemistry B, 2018, 6, 6615-6621.	5.8	38
138	Highly Efficient and Self-Standing Nanoporous NiO/Al <sub>3</sub> Ni <sub>2</sub> Electrocatalyst for Hydrogen Evolution Reaction. ACS Applied Energy Materials, 2019, 2, 7913-7922.	5.1	38
139	Development and Applications of Highly Functional Al-based Materials by Use of Metastable Phases. Materials Research, 2015, 18, 1414-1425.	1.3	37
140	Effects of hydrophobic layer on selective electrochemical nitrogen fixation of self-supporting nanoporous Mo4P3 catalyst under ambient conditions. Applied Catalysis B: Environmental, 2021, 286, 119895.	20.2	37
141	The nucleocapsid protein of SARS-associated coronavirus inhibits B23 phosphorylation. Biochemical and Biophysical Research Communications, 2008, 369, 287-291.	2.1	36
142	Effect of gas nitriding treatment on cavitation erosion behavior of commercially pure Ti and Tiâ^'6Alâ^'4V alloy. Surface and Coatings Technology, 2013, 221, 29-36.	4.8	36
143	Soluble interleukin-6 receptor is elevated during influenza A virus infection and mediates the IL-6 and IL-32 inflammatory cytokine burst. Cellular and Molecular Immunology, 2015, 12, 633-644.	10.5	36
144	Effect of porous NiTi alloy on bone formation: A comparative investigation with bulk NiTi alloy for 15Âweeks in vivo. Materials Science and Engineering C, 2008, 28, 1271-1275.	7.3	35

#	Article	IF	CITATIONS
145	Surface modification by gas nitriding for improving cavitation erosion resistance of CP-Ti. Applied Surface Science, 2014, 298, 164-170.	6.1	35
146	Novel deformation-induced polymorphic crystallization and softening of Al-based amorphous alloys. Acta Materialia, 2018, 147, 90-99.	7.9	35
147	Highly efficient amorphous np-PdFePC catalyst for hydrogen evolution reaction. Electrochimica Acta, 2019, 328, 135082.	5.2	35
148	The effects of a phytic acid/calcium ion conversion coating on the corrosion behavior and osteoinductivity of a magnesium-strontium alloy. Applied Surface Science, 2019, 484, 511-523.	6.1	35
149	Preparation of nickel-coated graphite by electroless plating under mechanical or ultrasonic agitation. Surface and Coatings Technology, 2014, 240, 425-431.	4.8	34
150	Nanoporous Nickel–Molybdenum Oxide with an Oxygen Vacancy for Electrocatalytic Nitrogen Fixation under Ambient Conditions. ACS Applied Materials & Interfaces, 2021, 13, 30722-30730.	8.0	34
151	Self-supported Ni(OH)2/MnO2 on CFP as a flexible anode towards electrocatalytic urea conversion: The role of composition on activity, redox states and reaction dynamics. Electrochimica Acta, 2019, 318, 32-41.	5.2	33
152	Low-cost fabrication of amorphous cobalt-iron-boron nanosheets for high-performance asymmetric supercapacitors. Electrochimica Acta, 2019, 296, 198-205.	5.2	33
153	Effect of Minor Sn Additions on the Formation and Properties of TiCuZrPd Bulk Glassy Alloy. Materials Transactions, 2012, 53, 500-503.	1.2	32
154	Al <sub>0.5</sub> TiZrPdCuNi High-Entropy (H-E) Alloy Developed through Ti <sub>20</sub> Zr <sub>20</sub> Pd <sub>20</sub> Cu <sub>20H-E Glassy Alloy Comprising Inter-Transition Metals. Materials Transactions, 2013, 54, 776-782.</sub>	t;Ni <su< td=""><td>b&amp;<b>gz</b>;20&lt;/s</td></su<>	b& <b>gz</b> ;20</s
155	Hierarchical Ni3S4@MoS2 nanocomposites as efficient electrocatalysts for hydrogen evolution reaction. Journal of Materials Science and Technology, 2021, 95, 70-77.	10.7	32
156	Eco-friendly and degradable red phosphorus nanoparticles for rapid microbial sterilization under visible light. Journal of Materials Science and Technology, 2021, 67, 70-79.	10.7	31
157	Theory-screened MOF-based single-atom catalysts for facile and effective therapy of biofilm-induced periodontitis. Chemical Engineering Journal, 2022, 431, 133279.	12.7	31
158	Oxygen Vacanciesâ€Rich Heterojunction of Ti <sub>3</sub> C <sub>2</sub> /BiOBr for Photoâ€Excited Antibacterial Textiles. Small, 2022, 18, e2104448.	10.0	31
159	Formation of bonelike apatite–collagen composite coating on the surface of NiTi shape memory alloy. Scripta Materialia, 2006, 54, 89-92.	5.2	30
160	Evolution of palladium/copper oxide–titanium dioxide nanostructures by dealloying and their catalytic performance for methanol electro-oxidation. Journal of Power Sources, 2015, 274, 1034-1042.	7.8	30
161	Design and synthesis of MWNTs-TiO 2 nanotube hybrid electrode and its supercapacitance performance. Journal of Power Sources, 2015, 283, 397-407.	7.8	30
162	Soft magnetic properties of Fe82-83B14-15Si2C0.5-1 amorphous alloys with high saturation magnetization above 1.7 T. Journal of Non-Crystalline Solids, 2018, 500, 173-180.	3.1	30

#	Article	IF	CITATIONS
163	A near infrared-activated photocatalyst based on elemental phosphorus by chemical vapor deposition. Applied Catalysis B: Environmental, 2019, 258, 117980.	20.2	30
164	Photo-controlled degradation of PLCA/Ti3C2 hybrid coating on Mg-Sr alloy using near infrared light. Bioactive Materials, 2021, 6, 568-578.	15.6	30
165	Glass-Forming Ability and Thermal Stability of Ti–Zr–Cu–Pd–Si Bulk Glassy Alloys for Biomedical Applications. Materials Transactions, 2007, 48, 163-166.	1.2	29
166	Synthesis and catalytic properties of Pd nanoparticles loaded nanoporous TiO2 material. Electrochimica Acta, 2013, 114, 35-41.	5.2	29
167	Pd-loaded In <sub>2</sub> O <sub>3</sub> nanowire-like network synthesized using carbon nanotube templates for enhancing NO <sub>2</sub> sensing performance. RSC Advances, 2015, 5, 30038-30045.	3.6	29
168	Electrodeposition of self-supported NiMo amorphous coating as an efficient and stable catalyst for hydrogen evolution reaction. Rare Metals, 2022, 41, 2624-2632.	7.1	29
169	One-step synthesis of petal-like apatite/titania composite coating on a titanium by micro-arc oxidation. Materials Letters, 2011, 65, 1041-1044.	2.6	28
170	Influence of ejection temperature on structure and glass transition behavior for Zr-based rapidly quenched disordered alloys. Acta Materialia, 2016, 116, 370-381.	7.9	28
171	3D Tungsten-Doped MoS <sub>2</sub> Nanostructure: A Low-Cost, Facile Prepared Catalyst for Hydrogen Evolution Reaction. Journal of the Electrochemical Society, 2016, 163, H299-H304.	2.9	28
172	One-step synthesis of size-controlled Br-doped TiO 2 nanoparticles with enhanced visible-light photocatalytic activity. Materials Research Bulletin, 2017, 86, 248-256.	5.2	28
173	Cobalt-iron (oxides) water oxidation catalysts: Tracking catalyst redox states and reaction dynamic mechanism. Journal of Catalysis, 2018, 365, 227-237.	6.2	28
174	Corrosion Behavior of Ti-Based Metallic Glasses. Materials Transactions, 2006, 47, 1934-1937.	1.2	27
175	Fe-based soft magnetic amorphous alloys with high saturation magnetization above 1.5ÂT and high corrosion resistance. Intermetallics, 2014, 54, 169-175.	3.9	27
176	Synthesis, characterization and biological evaluation of strontium/magnesium-co-substituted hydroxyapatite. Journal of Biomaterials Applications, 2016, 31, 140-151.	2.4	27
177	High-Frequency soft magnetic properties of Fe-Si-B-P-Mo-Cu amorphous and nanocrystalline alloys. Journal of Non-Crystalline Solids, 2019, 526, 119702.	3.1	27
178	A novel snail-inspired bionic design of titanium with strontium-substituted hydroxyapatite coating for promoting osseointegration. Journal of Materials Science and Technology, 2021, 79, 35-45.	10.7	27
179	Self-supported amorphous nanoporous nickel-cobalt phosphide catalyst for hydrogen evolution reaction. Progress in Natural Science: Materials International, 2021, 31, 201-206.	4.4	27
180	Formation of Ti-based bulk glassy alloy/hydroxyapatite composite. Scripta Materialia, 2008, 58, 287-290.	5.2	26

#	Article	IF	CITATIONS
181	Enhancement of gas-sensing abilities in p-type ZnWO4 by local modification of Pt nanoparticles. Analytica Chimica Acta, 2016, 927, 107-116.	5.4	26
182	Interface Polarization Strengthened Microwave Catalysis of MoS <sub>2</sub> /FeS/Rhein for the Therapy of Bacteriaâ€Infected Osteomyelitis. Advanced Functional Materials, 2022, 32, .	14.9	26
183	Improving the biocompatibility of NiTi alloy by chemical treatments: An in vitro evaluation in 3T3 human fibroblast cell. Materials Science and Engineering C, 2008, 28, 1117-1122.	7.3	25
184	A thick hierarchical rutile TiO2 nanomaterial with multilayered structure. Materials Research Bulletin, 2013, 48, 1961-1966.	5.2	25
185	Pyruvate Carboxylase Activates the RIG-I-like Receptor-Mediated Antiviral Immune Response by Targeting the MAVS signalosome. Scientific Reports, 2016, 6, 22002.	3.3	25
186	Peculiarities and usefulness of multicomponent bulk metallic alloys. Journal of Alloys and Compounds, 2017, 707, 12-19.	5.5	25
187	Nanoporous Palladium Hydride for Electrocatalytic N <sub>2</sub> Reduction under Ambient Conditions. Angewandte Chemie, 2020, 132, 3539-3544.	2.0	25
188	miR-21 promotes osseointegration and mineralization through enhancing both osteogenic and osteoclastic expression. Materials Science and Engineering C, 2020, 111, 110785.	7.3	25
189	Fe-B-Si-C-Cu amorphous and nanocrystalline alloys with ultrahigh hardness and enhanced soft magnetic properties. Journal of Non-Crystalline Solids, 2021, 554, 120606.	3.1	25
190	Spin State Tuning of the Octahedral Sites in Ni–Co-Based Spinel toward Highly Efficient Urea Oxidation Reaction. Journal of Physical Chemistry C, 2021, 125, 9190-9199.	3.1	25
191	Formation and characterization of iron oxide nanoparticles loaded on self-organized TiO2 nanotubes. Electrochimica Acta, 2010, 55, 5245-5252.	5.2	24
192	Characterization of self-organized TiO2 nanotubes on Ti–4Zr–22Nb–2Sn alloys and the application in drug delivery system. Journal of Materials Science: Materials in Medicine, 2011, 22, 461-467.	3.6	24
193	Preparation and Properties of Nanoâ€SiO2/Epoxy Composites Cured by Mannich Amine. Journal of Macromolecular Science - Physics, 2006, 45, 811-820.	1.0	23
194	Improvements in the Superelasticity and Change in Deformation Mode of β-Type TiNb24Zr2 Alloys Caused by Aging Treatments. Metallurgical and Materials Transactions A: Physical Metallurgy and Materials Science, 2011, 42, 2843-2849.	2.2	23
195	HCV NS4B induces apoptosis through the mitochondrial death pathway. Virus Research, 2012, 169, 1-7.	2.2	23
196	Preparation, Characterization and Mechanical Properties of Cu-Sn Alloy/Graphite Composites. Metallurgical and Materials Transactions A: Physical Metallurgy and Materials Science, 2014, 45, 5194-5200.	2.2	23
197	Inducible TAP1 Negatively Regulates the Antiviral Innate Immune Response by Targeting the TAK1 Complex. Journal of Immunology, 2017, 198, 3690-3704.	0.8	23
198	Accelerating the formation of a calcium phosphate layer on NiTi alloy by chemical treatments. Scripta Materialia, 2006, 54, 1457-1462.	5.2	22

#	Article	IF	CITATIONS
199	Preparation and electrocatalytic performance of nanoporous Pd/Sn and Pd/Sn-CuO composite catalysts. Electrochimica Acta, 2019, 296, 397-406.	5.2	22
200	In situ synthesis of exfoliation TiO2@C hybrids with enhanced photocatalytic hydrogen evolution activity. Applied Surface Science, 2020, 530, 147283.	6.1	22
201	Atomic-layer Fe2O3-modified 2D porphyrinic metal-organic framework for enhanced photocatalytic disinfection through electron-withdrawing effect. Applied Catalysis B: Environmental, 2022, 317, 121701.	20.2	22
202	Effects of Si addition on the glass-forming ability, glass transition and crystallization behaviors of Ti40Zr10Cu36Pd14 bulk glassy alloy. Intermetallics, 2008, 16, 609-614.	3.9	21
203	Synthesis, Characterization, and Biological Evaluation of Nanostructured Hydroxyapatite with Different Dimensions. Nanomaterials, 2017, 7, 38.	4.1	21
204	ZIF-67 derived Co@NC/g-C3N4 as a photocatalyst for enhanced water splitting H2 evolution. Environmental Research, 2021, 197, 111002.	7.5	21
205	Hierarchical nickle-iron layered double hydroxide composite electrocatalyst for efficient oxygen evolution reaction. Materials Today Nano, 2022, 17, 100150.	4.6	21
206	Optimizing the strontium content to achieve an ideal osseointegration through balancing apatite-forming ability and osteogenic activity. Materials Science and Engineering C, 2022, 133, 112647.	7.3	21
207	Ni- and Be-free Zr-based bulk metallic glasses with high glass-forming ability and unusual plasticity. Journal of the Mechanical Behavior of Biomedical Materials, 2012, 13, 166-173.	3.1	20
208	Material-herbology: An effective and safe strategy to eradicate lethal viral-bacterial pneumonia. Matter, 2021, 4, 3030-3048.	10.0	20
209	3D N-doped mesoporous carbon/SnO2 with polypyrrole coating layer as high-performance anode material for Li-ion batteries. Journal of Alloys and Compounds, 2022, 892, 162083.	5.5	20
210	Self-supporting nanoporous CoMoP electrocatalyst for hydrogen evolution reaction in alkaline solution. Journal of Colloid and Interface Science, 2022, 625, 606-613.	9.4	20
211	Pack cementation processing parameters for SiC coatings on C/C for optimum tribological properties. Surface and Coatings Technology, 2014, 254, 54-60.	4.8	19
212	Nanosized strontium substituted hydroxyapatite prepared from egg shell for enhanced biological properties. Journal of Biomaterials Applications, 2018, 32, 896-905.	2.4	19
213	Boosting oxygen reduction catalysis with abundant single atom tin active sites in zinc-air battery. Journal of Power Sources, 2021, 490, 229483.	7.8	19
214	Rutile-Coated B-Phase TiO <sub>2</sub> Heterojunction Nanobelts for Photocatalytic H <sub>2</sub> Evolution. ACS Applied Nano Materials, 2020, 3, 10349-10359.	5.0	18
215	Engineering Elastic Properties of Isostructural Molecular Perovskite Ferroelectrics via B‣ite Substitution. Small, 2021, 17, e2006021.	10.0	18
216	Synthesis of Br-doped TiO2 hollow spheres with enhanced photocatalytic activity. Journal of Nanoparticle Research, 2017, 19, 1.	1.9	17

#	Article	IF	CITATIONS
217	The Incorporation of Strontium in a Sodium Alginate Coating on Titanium Surfaces for Improved Biological Properties. BioMed Research International, 2017, 2017, 1-11.	1.9	17
218	Influence of Ag replacement on supercooled liquid region and icosahedral phase precipitation of Zr65Al7.5Ni10Cu17.5-xAgx (xÂ=Â0–17.5Âat%) glassy alloys. Journal of Alloys and Compounds, 2018, 735, 1712-1721.	5.5	17
219	"lmitative―click chemistry to form a sticking xerogel for the portable therapy of bacteria-infected wounds. Biomaterials Science, 2019, 7, 5383-5387.	5.4	17
220	Highly reversible electrochemical magnesium/lithium insertion performance in TiO2(B) nanosheets with Ti cationic vacancies. Chemical Engineering Journal, 2022, 442, 136146.	12.7	17
221	Electro-oxidation of ethylene glycol on nanoporous Ti–Cu amorphous alloy. Electrochimica Acta, 2011, 56, 10253-10258.	5.2	16
222	Anodization formation of through-hole nanoporous layers on TixNb1â^'x (x=0.3–0.7) alloys in nitric acid electrolytes. Applied Surface Science, 2012, 258, 3260-3263.	6.1	16
223	Extraordinary Supercapacitor Performance of a Multicomponent and Mixedâ€Valence Oxyhydroxide. Angewandte Chemie, 2015, 127, 8218-8222.	2.0	16
224	Four-electron oxygen reduction from mesoporous carbon modified with Fe2O3 nanocrystals. Journal of Materials Science, 2017, 52, 10938-10947.	3.7	16
225	Dual-phase nanostructuring as a route to flexible nanoporous metals with outstanding comprehensive mechanical properties. Science China Materials, 2021, 64, 2289-2304.	6.3	16
226	Nanoporous Ni/NiO catalyst for efficient hydrogen evolution reaction prepared by partial electro-oxidation after dealloying. Journal of Alloys and Compounds, 2022, 911, 165061.	5.5	16
227	Synthesis of Ti-Based Glassy Alloy/Hydroxyapatite Composite by Spark Plasma Sintering. Materials Transactions, 2008, 49, 502-505.	1.2	15
228	Zr-based bulk metallic glass composite with in situ precipitated nanocrystals. Journal of Alloys and Compounds, 2014, 586, 155-158.	5.5	15
229	Effect of atomic structure on preferential oxidation of alloys: amorphous versus crystalline Cu-Zr. Journal of Materials Science and Technology, 2020, 40, 128-134.	10.7	15
230	Amorphous CoMoO <sub>4</sub> with Nanoporous Structures for Electrochemical Ammonia Synthesis under Ambient Conditions. ACS Sustainable Chemistry and Engineering, 2020, 8, 19072-19083.	6.7	15
231	Formation, thermal stability and mechanical properties of high-entropy (Fe0.25Co0.25Ni0.25Cr0.125Mo0.0625Nb0.0625)100‒Bx (xÂ= 7–14) amorphous alloys. Journal of Alloys a Compounds, 2020, 825, 153858.	nd5.5	15
232	Understanding the macroscopical flexibility/fragility of nanoporous Ag: Depending on network connectivity and micro-defects. Journal of Materials Science and Technology, 2020, 53, 91-101.	10.7	15
233	Facile synthesis of defected TiO2- (B) nanosheet/graphene oxide hybrids with high photocatalytic H2 activity. Journal of Materials Science and Technology, 2021, 80, 171-178.	10.7	15
234	Self-standing nanoporous NiPd bimetallic electrocatalysts with ultra-low Pd loading for efficient hydrogen evolution reaction. Electrochimica Acta, 2022, 411, 140077.	5.2	15

#	Article	IF	CITATIONS
235	Recent progress of photo-excited antibacterial materials via chemical vapor deposition. Chemical Engineering Journal, 2022, 437, 135401.	12.7	15
236	Effects of growing integrated layer [GIL] formation on bonding behavior between hydroxyapatite ceramics and Ti-based bulk metallic glasses via hydrothermal hot-pressing. Materials Science and Engineering B: Solid-State Materials for Advanced Technology, 2009, 161, 27-30.	3.5	14
237	Effect of cobalt microalloying on the glass forming ability of Ti–Cu–Pd–Zr metallic glass. Journal of Non-Crystalline Solids, 2013, 379, 155-160.	3.1	14
238	The fabrication of SnSe/Ag nanoparticles on TiO2 nanotubes. Materials Science and Engineering B: Solid-State Materials for Advanced Technology, 2013, 178, 77-82.	3.5	14
239	Gene Expression and Antiviral Activity of Interleukin-35 in Response to Influenza A Virus Infection. Journal of Biological Chemistry, 2016, 291, 16863-16876.	3.4	14
240	Self-supporting CoMoC nanoporous catalysts for N2 reduction reaction under ambient conditions. Applied Surface Science, 2020, 521, 146385.	6.1	14
241	Photothermal-controlled sustainable degradation of protective coating modified Mg alloy using near-infrared light. Rare Metals, 2021, 40, 2538-2551.	7.1	14
242	Effect of TiO2 Nanotube Morphology on the Formation of Apatite Layer in Simulated Body Fluid. Current Nanoscience, 2010, 6, 256-261.	1.2	13
243	Preparation of Nanoporous Pd/CuO by Dealloying and Their Electrocatalysis for Methanol in Alkaline Condition. Journal of the Electrochemical Society, 2014, 161, F1474-F1480.	2.9	13
244	In vivo evaluation of a Ti-based bulk metallic glass alloy bar. Bio-Medical Materials and Engineering, 2015, 26, 9-17.	0.6	13
245	Cytotoxicity and antibacterial efficacy of silver nanoparticles deposited onto dopamine-functionalised titanium. Materials Express, 2015, 5, 191-200.	0.5	13
246	Amorphous FeNiNbPC nanoprous structure for efficient and stable electrochemical oxygen evolution. Journal of Colloid and Interface Science, 2022, 608, 1973-1982.	9.4	13
247	Formation, microstructure and mechanical properties of ductile Zr-rich Zr–Cu–Al bulk metallic glass composites. Journal of Materials Research and Technology, 2021, 15, 5452-5465.	5.8	13
248	Photo-excited antibacterial poly(ƕcaprolactone)@MoS2/ZnS hybrid nanofibers. Chemical Engineering Journal, 2022, 434, 134764.	12.7	13
249	Nanoâ€ <b>s</b> iO <sub>2</sub> Doped Polystyrene Materials for Inertial Confinement Fusion Targets. Journal of Macromolecular Science - Physics, 2005, 44, 237-248.	1.0	12
250	Effect of hydroxyapatite content on the microstructure, thermal and mechanical properties of Ti-based glassy alloy/hydroxyapatite composite prepared by spark plasma sintering. Intermetallics, 2011, 19, 572-576.	3.9	12
251	Anatase TiO 2 hierarchical nanospheres with enhanced photocatalytic activity for degrading methyl orange. Materials Chemistry and Physics, 2016, 170, 186-192.	4.0	12
252	Development of a more efficient hepatitis B virus vaccine by targeting hepatitis B virus preS to dendritic cells. Vaccine, 2016, 34, 516-522.	3.8	12

#	Article	IF	CITATIONS
253	Synthesis of rutile–brookite TiO 2 by dealloying Ti–Cu amorphous alloy. Materials Research Bulletin, 2016, 73, 290-295.	5.2	12
254	Free-standing ternary NiWP film for efficient water oxidation reaction. Applied Surface Science, 2018, 434, 871-878.	6.1	12
255	On the competition between synchronous oxidation and preferential oxidation in Cu-Zr-Al metallic glasses. Corrosion Science, 2020, 177, 108996.	6.6	12
256	Rapid and highly effective bacteria-killing by polydopamine/IR780@MnO2–Ti using near-infrared light. Progress in Natural Science: Materials International, 2020, 30, 677-685.	4.4	12
257	Insight into the electrochemical-cycling activation of Pt/molybdenum carbide toward synergistic hydrogen evolution catalysis. Journal of Catalysis, 2020, 384, 169-176.	6.2	12
258	Highly flexible and conductive nanoporous Ag as good substrate for flexible hybrid supercapacitors. Journal of Alloys and Compounds, 2021, 854, 157095.	5.5	12
259	Highly durable Cu–N–C active sites towards efficient oxygen reduction for zinc-air battery: Carbon matrix effect, reaction mechanism and pathways. Journal of Alloys and Compounds, 2021, 857, 158321.	5.5	12
260	Microstructure and Corrosion Resistance of Ti–Zr–Cu–Pd–Sn Glassy and Nanocrystalline Alloys. Materials Transactions, 2007, 48, 167-170.	1.2	11
261	Influence of temperature on viscous flow deformation of Zr55Cu30Al10Ni5 bulk glassy alloy in supercooled liquid region. Intermetallics, 2007, 15, 885-890.	3.9	11
262	Bioactivity of titanium-based bulk metallic glass surfaces via hydrothermal hot-pressing treatment. Journal of the Ceramic Society of Japan, 2008, 116, 115-117.	1.1	11
263	Novel nanosized anatase TiO2 hexagonal prism filled with nanoporous structure. Materials and Design, 2017, 116, 238-245.	7.0	11
264	Specific Emitter Identification Based on the Natural Measure. Entropy, 2017, 19, 117.	2.2	11
265	Enhancement of photocatalytic H2 production by metal complex electrostatic adsorption on TiO2 (B) nanosheets. Journal of Materials Chemistry A, 2019, 7, 3797-3804.	10.3	11
266	Thermal oxidation of amorphous Cu Zr1â^ alloys: Role of composition-dependent thermodynamic stability. Applied Surface Science, 2020, 503, 144376.	6.1	11
267	Tuning cobalt eg occupation of Co-NCNT by manipulation of crystallinity facilitates more efficient oxygen evolution and reduction. Journal of Catalysis, 2020, 383, 221-229.	6.2	11
268	Using tea nanoclusters as β-lactamase inhibitors to cure multidrug-resistant bacterial pneumonia: A promising therapeutic strategy by Chinese materioherbology. Fundamental Research, 2022, 2, 496-504.	3.3	11
269	Stress corrosion cracking and bioactivity of Ti-based bulk metallic glass. Journal of Alloys and Compounds, 2014, 615, S123-S127.	5.5	10
270	Effect of Na+ and NaOH concentrations on the surface morphology and dissolution behavior of hydroxyapatite. Ceramics International, 2015, 41, 3461-3468.	4.8	10

#	Article	IF	CITATIONS
271	Nanocrystal Bismuth Telluride Electrocatalysts for Highly Efficient Oxygen Reduction. Journal of the Electrochemical Society, 2015, 162, H785-H791.	2.9	10
272	Effects of both Sr and Mg substitution on compositions of biphasic calcium phosphate derived from hydrothermal method. International Journal of Applied Ceramic Technology, 2018, 15, 210-222.	2.1	10
273	Controlled and sustained drug release performance of calcium sulfate cement porous TiO <sub>2</sub> microsphere composites. International Journal of Nanomedicine, 2018, Volume 13, 7491-7501.	6.7	10
274	Tuning the ï€-electron delocalization degree of mesoporous carbon for hydrogen peroxide electrochemical generation. Journal of Catalysis, 2020, 392, 1-7.	6.2	10
275	Influences of strontium on the phase composition and lattice structure of biphasic calcium phosphate. Ceramics International, 2021, 47, 16248-16255.	4.8	10
276	Surface photodynamic ion sterilization of ITO-Cu2O/ZnO preventing touch infection. Journal of Materials Science and Technology, 2022, 122, 10-19.	10.7	10
277	Preparation and Characterization of Nanoâ€īiO2 Doped Polystyrene Materials by Melt Blending for Inertial Confinement Fusion. Journal of Macromolecular Science - Physics, 2004, 43, 871-882.	1.0	9
278	Self-organized nanotubular layer on Ti–4Zr–22Nb–2Sn alloys formed in organic electrolytes. Journal of Materials Research, 2009, 24, 3647-3652.	2.6	9
279	Study on the formation micromechanism of TiO2 nanotubes on pure titanium and the role of fluoride ions in electrolyte solutions. Thin Solid Films, 2011, 519, 5150-5155.	1.8	9
280	Facile In Situ Hydrothermal Method for Synthesis of SrTiO <sub>3</sub> /TiO <sub>2</sub> Nanostructures with Improved Photoelectrochemical Activities. Journal of the Electrochemical Society, 2013, 160, H704-H709.	2.9	9
281	Ti Particles Dispersed Ti-Based Metallic Glass Matrix Composite Prepared by Spark Plasma Sintering. Materials Transactions, 2013, 54, 1335-1338.	1.2	9
282	Fabrication, characterization, and photocatalytic properties of anatase TiO2 nanoplates with exposed {001} facets. Journal of Nanoparticle Research, 2014, 16, 1.	1.9	9
283	Sub-Tg relaxation and multi-stage glass transition behavior for bulk glassy alloys. Journal of Alloys and Compounds, 2015, 643, S11-S16.	5.5	9
284	Synthesis of TiO2Nanoparticles Loaded Pd/CuO Nanoporous Catalysts and Their Catalytic Performance for Methanol, Ethanol and Formic Acid Electro-Oxidations. Journal of the Electrochemical Society, 2016, 163, E263-E271.	2.9	9
285	SENNTIX-type amorphous alloys with high B s and improved corrosion resistance. Journal of Alloys and Compounds, 2017, 707, 195-198.	5.5	9
286	Liquid ejection temperature dependence of structure and glass transition behavior for rapidly solidified Zr-Al-M (M=Ni, Cu or Co) ternary glassy alloys. Journal of Alloys and Compounds, 2018, 739, 1104-1114.	5.5	9
287	Multicomponent bulk metallic glasses with elevated-temperature resistance. MRS Bulletin, 2019, 44, 867-872.	3.5	9
288	Unveiling the roles of multiple active sites during oxygen reduction reaction in Cr2O3@Cr-N-C composite catalyst. Journal of Catalysis, 2021, 396, 402-408.	6.2	9

#	Article	IF	CITATIONS
289	Large-Scale Synthetic Graphene on Cu as Anti-Corrosion Coating by Chemical Vapor Deposition Approach. Science of Advanced Materials, 2014, 6, 545-549.	0.7	9
290	Inducible CYP4F12 enhances Hepatitis C virus infection via association with viral nonstructural protein 5B. Biochemical and Biophysical Research Communications, 2016, 471, 95-102.	2.1	8
291	Influence of Ag replacement on the formation and heating-induced phase decomposition of Zr65Al7.5Co27.5-xAgx (x=5 to 20†at%) glassy alloys. Journal of Alloys and Compounds, 2019, 783, 545-554.	5.5	8
292	Preparation of nanoporous Sn-doped TiO2 anode material for lithium-ion batteries by a simple dealloying method. Ionics, 2020, 26, 4363-4372.	2.4	8
293	Microstructure and mechanical properties of TC4 joints brazed with Ti–Zr–Cu–Sn amorphous filler alloy. Rare Metals, 2021, 40, 1881-1889.	7.1	8
294	Corrosion resistance of pseudo-high entropy Fe-containing amorphous alloys in chloride-rich media. Journal of Alloys and Compounds, 2021, 884, 161090.	5.5	8
295	Modulate the superficial structure of La2Ce2O7 catalyst with anchoring CuO species for the selective catalytic oxidation of NH3. Journal of Materials Science and Technology, 2022, 111, 1-8.	10.7	8
296	A smart strategy of "laser-direct-writing―to achieve scalable fabrication of self-supported MoNi <sub>4</sub> /Ni catalysts for efficient and durable hydrogen evolution reaction. Journal of Materials Chemistry A, 2022, 10, 12722-12732.	10.3	8
297	Effects of Minor Si Addition on Glass Formation and Thermal Stability of Ni Free Ti-Based Bulk Metallic Glass. Materials Science Forum, 2013, 750, 36-39.	0.3	7
298	Incomplete phase-space method to reveal time delay from scalar time series. Physical Review E, 2016, 94, 052210.	2.1	7
299	The Large Scale Synthesis of Aligned Plate Nanostructures. Scientific Reports, 2016, 6, 29972.	3.3	7
300	Numerical study on the self-heating effects for vacuum/high-k gate dielectric tri-gate FinFETs. Microelectronics Reliability, 2019, 95, 52-57.	1.7	7
301	Formation, structure and properties of pseudo-high entropy clustered bulk metallic glasses. Journal of Alloys and Compounds, 2020, 820, 153164.	5.5	7
302	Icosahedral and dodecagonal quasicrystal plus glass alloys with plastic deformability. Acta Materialia, 2020, 199, 1-8.	7.9	7
303	High-temperature oxidation behaviour of refurbished (Ni,Pt)Al coating on Ni-based superalloy at 1100 °C. Corrosion Science, 2021, 187, 109521.	6.6	7
304	Temperature-Time-Transformation Curve and Viscous Flow Deformation of Zr <sub>55</sub> Cu <sub>30</sub> Al <sub>10</sub> Ni <sub>5</sub> Bulk Glassy Alloy. Materials Transactions, 2006, 47, 2308-2311.	1.2	6
305	Formation of Ca–P layer on the Ti-based bulk glassy alloy by chemical treatment. Journal of Alloys and Compounds, 2010, 504, S168-S171.	5.5	6
306	CdS sensitized nanoporous TiO2/CuO layer prepared by dealloying of Ti–Cu amorphous alloy. Materials Letters, 2012, 80, 131-134.	2.6	6

#	Article	IF	CITATIONS
307	Solution Process for Synthesizing Bioactive Nano-Mesh Layer on Ti-Based Bulk Metallic Glasses. Materials Transactions, 2013, 54, 1343-1346.	1.2	6
308	The controllable preparation of Co3O4 nanostructure for designing optimal mechanical and magnetic properties of graphite/kaolin based compounds. Materials and Design, 2018, 143, 169-176.	7.0	6
309	Synthesis of polyaluminocarbosilane with low branched molecular structure using liquid polysilacarbosilane and aluminum acetylacetonate by highâ€pressure method. Applied Organometallic Chemistry, 2019, 33, e4720.	3.5	6
310	Preparation and physicochemical properties of an injectable alginate-based hydrogel by the regulated release of divalent ions via the hydrolysis of <scp>d</scp> -glucono- <b>δ</b> -lactone. Journal of Biomaterials Applications, 2020, 34, 891-901.	2.4	6
311	Activity descriptor identification for hydrogen evolution reaction on well-dispersed few layer MoS2(O) nanosheets over the mesoporous carbonic arrays. Journal of Alloys and Compounds, 2020, 842, 155744.	5.5	6
312	Zr55Al10Ni5Cu30 amorphous alloy film prepared by magnetron sputtering method. Rare Metals, 2021, 40, 2237-2243.	7.1	6
313	Revealing the univariate effect of structural order on the oxidation of ternary alloys: Amorphous vs. crystalline Cu–Zr–Al alloys. Corrosion Science, 2021, 183, 109309.	6.6	6
314	Enhanced Electrocatalysis for Hydrogen Evolution over a Nanoporous NiAlTi/Al <sub>3</sub> Ti Hybrid. ACS Applied Energy Materials, 2021, 4, 7579-7588.	5.1	6
315	Plastic Zr-Al-Ni-Cu-Ag bulk glassy alloys containing quasicrystalline or β-Zr plus ω-Zr phases. Acta Materialia, 2022, 229, 117812.	7.9	6
316	Effect of Minor Addition Ta on the Thermal Stability and Corrosion Resistance of Ti-Zr-Cu-Pd Bulk Metallic Glasses. Materials Science Forum, 2013, 750, 23-26.	0.3	5
317	Microstructure and Cavitation Erosion Properties of Ceramic Coatings Fabricated on Ti-6Al-4V Alloy by Pack Carburizing. Journal of Materials Engineering and Performance, 2014, 23, 2772-2779.	2.5	5
318	The morphology control and mechanical properties of nanoporous Ag. Materials and Design, 2020, 192, 108741.	7.0	5
319	Novel heating- and deformation-induced phase transitions and mechanical properties for multicomponent Zr50M50, Zr50(M,Ag)50 and Zr50(M,Pd)50 (MÂ=ÂFe,Co,Ni,Cu) amorphous alloys. Journal of Materials Science and Technology, 2022, 104, 109-118.	10.7	5
320	Citric acid and lactic acid have a synergetic effect on absorbing the bone mineral crystal. Materials Letters, 2018, 215, 218-220.	2.6	4
321	Photocatalysis: Lightâ€Activated Rapid Disinfection by Accelerated Charge Transfer in Red Phosphorus/ZnO Heterointerface (Small Methods 3/2019). Small Methods, 2019, 3, 1970008.	8.6	4
322	Production of Bulk Glassy Alloy Parts by a Levitation Melting-Forging Method. Materials Transactions, 2006, 47, 2072-2075.	1.2	3
323	The Influence of Viscous Flow Deformation on the Thermal Stability and Hardness of ZrCuAlNi Bulk Glassy Alloy. Materials Transactions, 2007, 48, 1748-1751.	1.2	3
324	Interface Structure between Ti-Based Bulk Metallic Glasses and Hydroxyapatite Ceramics Jointed by Hydrothermal Techniques. Materials Transactions, 2009, 50, 1308-1312.	1.2	3

#	Article	IF	CITATIONS
325	Microstructure and Electrochemical Behavior of Pd–Cu–Ni–P Bulk Metallic Glass and Its Crystallized Alloys. Materials Transactions, 2012, 53, 936-939.	1.2	3
326	SnSe Nanoparticles Anchored on TiO2 Nanotube Arrays by Pulsed Electrochemical Deposition. Electrochemical and Solid-State Letters, 2012, 15, D4.	2.2	3
327	Ti-Based Bulk Metallic Glass Composites Produced by Spark Plasma Sintering. Materials Science Forum, 2013, 750, 52-55.	0.3	3
328	Electrochemical Properties of Porous Pd-Based Bulk Metallic Glasses. Materials Transactions, 2013, 54, 1347-1350.	1.2	3
329	Synthesis and photocatlytic performance of nano-sized TiO2 materials prepared by dealloying Ti–Cu–Pd amorphous alloys. Materials Research Bulletin, 2015, 65, 302-306.	5.2	3
330	Specific Emitter Identification Based on Visibility Graph Entropy. Chinese Physics Letters, 2018, 35, 030501.	3.3	3
331	Phase decomposition and mechanical properties of pseudo-high entropy Zr65(Al,Fe,Co,Ni,M)35 (M=Cu,) Tj ETQq1	10.7843 5.5	14 rgBT /0
332	A self-supported FeNi layered double hydroxide anode with high activity and long-term stability for efficient oxygen evolution reaction. Sustainable Energy and Fuels, 2021, 5, 3205-3212.	4.9	3
333	Carbon-Assistant Nanoporous Gold for Surface-Enhanced Raman Scattering. Nanomaterials, 2022, 12, 1455.	4.1	3
334	Zr-rich Zr-Al-Ni-Ag metallic glass composites with high strength and plastic strain. Journal of Alloys and Compounds, 2022, 918, 165683.	5.5	3
335	Bioactive NiTi Implants Used for Bone Repairing Applications. Key Engineering Materials, 2005, 288-289, 599-602.	0.4	2
336	Effects of femtosecond laser ablation on the surface morphology and microstructure of a bulk TiCuPdZr glass alloy. Rare Metals, 2009, 28, 272-276.	7.1	2
337	Corrosion Behavior of Porous Ti-24Nb-4Zr Alloy in Different Simulated Body Fluids. Advanced Materials Research, 0, 399-401, 1577-1581.	0.3	2
338	Kinetics of Passive Film on Low Carbon Steel in Sodium Nitrate Solution by Numerical Analysis Method. Advanced Materials Research, 2012, 457-458, 358-364.	0.3	2
339	Fabrication of a Ternary Hybrid Semiconductor ZnFe2O4/CdS-TiO2 NTs Structure on the Ti-5Zr Alloy. Current Nanoscience, 2012, 8, 643-650.	1.2	2
340	AG NANOPARTICLES-MODIFIED ANATASE <font>TiO</font> <sub>2</sub> SINGLE CRYSTALS CUBES FOR IMPROVING PHOTOELECTRIC CONVERSION. Nano, 2014, 09, 1450012.	1.0	2
341	Multilayer modification on titanium surface for in situ delivery of MicroRNAs. Materials Letters, 2014, 133, 243-246.	2.6	2
342	Synthesis of self-detached nanoporous titanium-based metal oxide. Journal of Solid State Chemistry, 2015, 229, 78-86.	2.9	2

#	Article	IF	CITATIONS
343	Preparation of hydroxyapatite layer on Ti-based bulk metallic glasses by acid and alkali pre-treatment. Rare Metals, 2015, 34, 22-27.	7.1	2
344	Preparation and electrocatalytic performance of the Pt supported on the alkali-treated nanoporous TiO2 material. Ionics, 2015, 21, 2863-2869.	2.4	2
345	Annealing-induced enthalpy relaxation behavior of Ni-Pd-P-B bulk glassy type alloys. Materials Science & Engineering A: Structural Materials: Properties, Microstructure and Processing, 2016, 674, 250-255.	5.6	2
346	Photocatalytic Performance of Ag Nanoparticles Modified ZnO Microplates Prepared by One-Step Method. Current Nanoscience, 2014, 10, 389-393.	1.2	2
347	Growth direction dependent separate-channel charge transport in the organic weak charge-transfer co-crystal of anthracene–DTTCNQ. Materials Horizons, 2022, , .	12.2	2
348	Enhancement of Corrosion Resistance of Titanium-Copper Based Metallic Glass by Methylsiloxane Coating. Materials Transactions, 2009, 50, 1334-1339.	1.2	1
349	Effects of pulse voltage on the formation of nanoporous Ti oxides by dealloying amorphous TiCu alloy. Journal of Physics: Conference Series, 2013, 417, 012022.	0.4	1
350	Periodic corrugation on fracture surface of Zr-based bulk metallic glass composite with in situ precipitated nanocrystalloids. , 2013, , .		1
351	Formation, characterization, and properties of radiopaque TaC–C/C and ZrO <sub>2</sub> –C/C composites. Materials Express, 2015, 5, 518-526.	0.5	1
352	Syntheses and Fundamental Properties of Fe-rich Metastable Phase Alloys with Saturation Magnetization Exceeding 1.9 T. Materials Research, 2015, 18, 127-135.	1.3	1
353	Specific emitter identification based on horizontal visibility graph. , 2017, , .		1
354	Ultrahigh thermal stability and hardness of nano-mixed fcc-Al and amorphous phases for multicomponent Al-based alloys. Journal of Alloys and Compounds, 2020, 832, 154997.	5.5	1
355	Hydrothermal Synthesis of CdS Layer on Ag Nanowires and its Enhanced Photocatalytic Activity. Current Nanoscience, 2015, 11, 633-639.	1.2	1
356	A Three-Dimensional Cement Quantification Method for Decision Prediction of Vertebral Recompression after Vertebroplasty. Computational and Mathematical Methods in Medicine, 2022, 2022, 1-14.	1.3	1
357	Study on a Quinoline Inhibitor Used for Sulfur Corrosion on Carbon Steel: Properties Research and Field Test. Advanced Materials Research, 2011, 337, 106-111.	0.3	0
358	The Porous TiNb <sub>24</sub> Zr <sub>4</sub> Alloys with Controllable Porosity Fabricated by Conventional Sintering. Advanced Materials Research, 0, 335-336, 797-804.	0.3	0
359	Effect of SO42â^' on microstructure, phase and photocatalytic activity of TiO2 nanomaterials prepared from Ti–Cu amorphous alloy. Materials Research Innovations, 2014, 18, S4-728-S4-733.	2.3	0
360	Enhanced Capacitance of TiO <sub>2</sub> Single Crystals Through Chemically Deposited Graphene Films. Journal of Nanoscience and Nanotechnology, 2015, 15, 4567-4573.	0.9	0

#	Article	IF	CITATIONS
361	Syntheses and Fundamental Properties of Cr/Mo-Adoped Fe-Rich Alloys With Metastable Phase and Saturation Magnetization Near 1.9 T. Materials Research, 2016, 19, 1299-1303.	1.3	Ο
362	Correlation between Mechanical Strength of Amorphous TiO <sub>2</sub> Nanotubes and Their Solid State Crystallization Pathways. ChemistrySelect, 2018, 3, 10711-10716.	1.5	0
363	Features and Prospects of Multicomponent Metallic Glasses. Funtai Oyobi Fummatsu Yakin/Journal of the Japan Society of Powder and Powder Metallurgy, 2018, 65, 37-44.	0.2	0
364	Chaos Identification Based on Component Reordering and Visibility Graph. Chinese Physics Letters, 2017, 34, 050501.	3.3	0